Annuaire de l'Universite "St. Kliment Ohridski", Faculte de Physique, 99, 2006

PERFORMANCE OF THE RESISTIVE PLATE CHAMBERS OF THE HARP EXPERIMENT

MARIYAN BOGOMILOV, DIMITAR KOLEV, ROUMEN TSENOV

Department of Atomic Physics

Мариян Богомилов, Димитър Колев, Румен Ценов. ХАРАКТЕРИСТИКИ НА КАМЕРИТЕ СЪС СЪПРОТИВИТЕЛНИ ПЛОСКОСТИ В ЕКСПЕРИМЕНТА HARP

Описана е система от газови детектори на елементарни частици, наричани камери със съпротивителни плоскости (RPC), използвани за идентификация на заредени лептони и адрони по времето им на прелитане. Те са част от експеримента HARP в Европейския център за ядрени изследвания CERN в Женева, Швейцария. В тази работа са дадени геометрията на камерите и техните цели. В детайли са описани характеристиките, разработената калибровъчна процедура и възможностите на RPC да идентифицират частиците.

Mariyan Bogomilov, Dimitar Kolev, Roumen Tsenov. PERFORMANCE OF THE RESISTIVE PLATE CHAMBERS OF THE HARP EXPERIMENT

We describe a system of gaseous detectors of elementary particles, called Resistive Plate Chambers (RPC) used for identification of charged leptons and hadrons by time-of-flight. They are a part of the HARP experiment at European Organization for Nuclear Research CERN in Geneva, Switzerland. The geometry of chambers and their aims are given in this article. The performance, the developed calibration procedure and particle identification capability of RPC are described in details.

Keywords: resistive plate chamber, RPC, TOF, HARP, gaseous detector
PACS numbers: 07.77.Ka; 29.40.-n; 29.40.Cs; 82.80.Rt

1. INTRODUCTION

The HARP experiment is performing measurement of hadron production cross-section on fixed targets over almost full solid angle with precision of few percent [1]. A wide range of target materials and thicknesses is exposed on beams of protons and pions with momenta between 2 and 15 GeV/c. The HARP experiment is located at T9 beam line at the Proton Synchrotron at CERN. From August 2001 to October 2002 HARP takes 450 million physics triggers, collects data for about 300 different settings and records more than 30 TB information. The main motivations for building of HARP are four:

1. Measuring low energy hadron production for targets relevant to design of future neutrino facilities such as neutrino factory or muon colliders.
2. Measuring the hadron fluxes in the atmosphere coming from collisions of protons with atmospheric nuclei and resulting in atmospheric neutrino fluxes.
3. Measuring hadron fluxes with high accuracy needed for existing neutrino experiments K2K [2] and MiniBooNE [3].
4. The measurement of cross-sections will be used for improvement of current hadron generators. HARP will serve mainly GEANT4 Collaboration [4].

The setup of the HARP spectrometer is shown in Fig. 1. It can be divided into three subsystems:

- *Beam and trigger detectors* (not shown in the sketch) provide identification, reconstruction of beam particles and trigger decision. The devices are:

  Two *Cherenkov Counters* are for particle identification. They operated in threshold mode and the gas pressure is adjusted according to the beam momentum and the tagged particles.

  Four *Multi-Wire Proportional Chambers* are used for tracking of the beam particles and for monitoring of the beam profile and position. They measure track parameters and define the impact point of the beam particle with the target.

  The *Time-Of-Flight (TOF)* detector consists of two scintillator strip hodoscopes. They identify incoming beam particles by measuring the time of particle to traverse 21.4 m distance between the scintillators. It is complementary to Cherenkov Counters in low momenta.

  Two *Halo Scintillators* reject the events when a beam particle is present in the beam halo.

  Beam Scintillator starts the trigger decision, *i.e.*, the first trigger signal,

when there is a coincident with a signal in the TOF scintillators.
Target Defining Scintillator is located as near as possible to the target and it generates signal for accepting the event if it is hit by a beam particle. The efficiency is very high (> 99.9%):
Inner Trigger Cylinder surrounds the target and triggers on secondaries emanated from the target at large angles with respect to beam direction. It is made by scintillating fibres.
Forward Trigger Plane is complementary to Inner Trigger Cylinder and covers the small angles. It is also made by scintillator slabs.

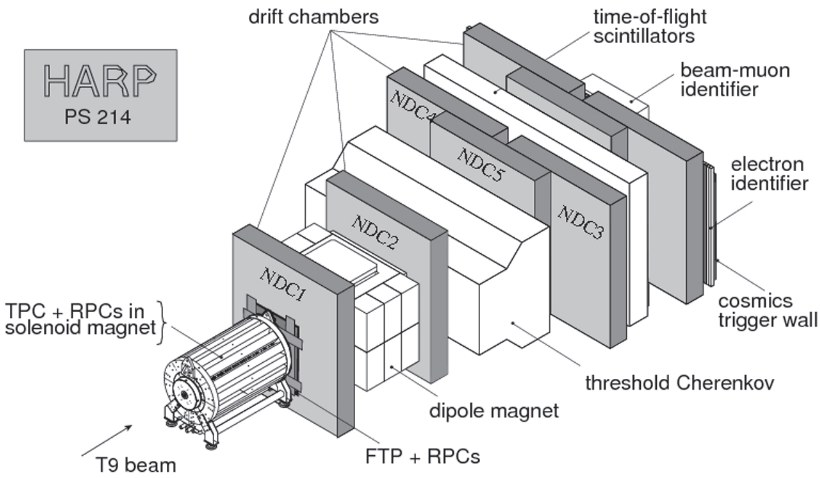

Fig. 1. Layout of the HARP experiment

- *Large angle detectors* provide identification and tracking of secondaries at angles larger than 20°. There are two detectors included:
  Time Projection Chamber (TPC) is a cylinder with length of 150 cm and diameter of 80 cm. The TPC is located inside a solenoid magnet surrounding the target. The active volume is fill with a gas mixture in which secondary particles bend its trajectory in the magnetic field, ionizing the gas molecules. The ions drift to the corresponding electrodes due to applied high voltage with gradient parallel to the TPC cylinder axis of symmetry (beam direction). In this way TPC measures the momentum, position and energy (ionizing) losses of the particle.
  Resistive Plate Chambers are the topic of this article. Their detailed description is in the next sections.
- *Forward detectors* cover tracking and identification at small production angles. The detectors are:

20 *Drift Chambers* are arranged in five modules. They measure track parameters and momentum of secondary particles at small angles with respect to the beam axis. The presence of the curvature of the track in the forward regions is due to a dipole magnet (see Fig. 1).
Cherenkov Counter distinguishes secondary particles at high momenta. It also works in threshold mode at atmospheric pressure.
Time-Of-Flight (TOF) Wall is a set of scintillators which identify particles at low energies complementary to Cherenkov Counter. The path of the flight from the target to the TOF Wall is about 10 m.
e and μ identifier discriminates electrons and muons from light hadrons. It is made as a "sandwich" structure from scintillators, iron and lead plates.

2. OVERVIEW OF THE HARP RESISTIVE PLATE CHAMBERS

The resistive plate chamber system (RPC) is a part of the large-angle HARP spectrometer and consist of a set of 16 vertical chambers, called forward RPC plane and another set of 30 chambers grouped in a cylindrical arrangement and named barrel RPC. The total number of RPC channels[1] is 368; 8 channels per chamber; 240 channels in the barrel and 128 in the forward RPC plane. In Fig. 2. schematic view of the barrel RPCs is shown. More information about geometry and construction can be found in [5].

The main goal of the RPC is identification of particles with momenta of a few hundred MeV/c in the medium and large angle regions via time-of-flight. The RPCs cover a phase space where the TPC cannot distinguish particles by multiple energy loss measurements: electrons/pions (100–250 MeV/c); electrons/kaons (~ 500 MeV/c) and pions/protons (~ 1 GeV/c).

In order to calibrate RPC and demonstrate the performance a large subset of accumulated statistics is used. The amount of reconstructed events used for the calibration purpose is approximately 8 million. It covers Cu, Sn, Ta, and Pb targets, all with a thickness of 5% of an interaction length, exposed to 3 GeV/c, 5 GeV/c, and 8 GeV/c beams of positive particles (pions, protons). The procedure described here is available as code and released as part of the public HARP software.

[1] Sometimes we refer to them as 'RPC pads'.

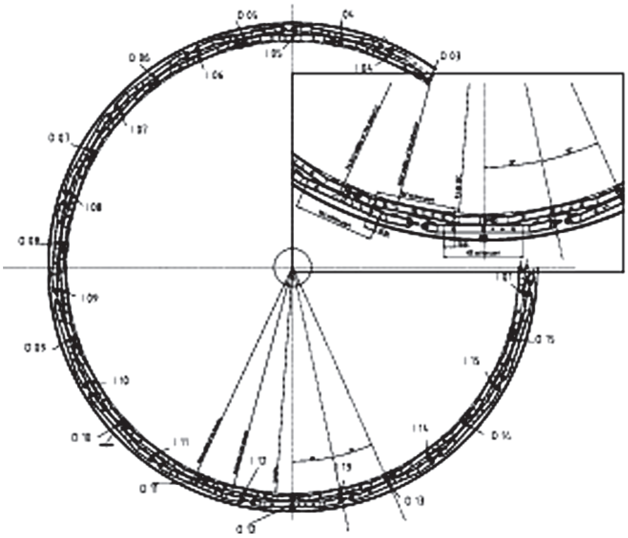

Fig. 2. Schematic layout of the barrel RPC (*x-y* plane, perpendicular to the beam) of the barrel RPC set. It comprises 30 chambers in two layers, surrounding TPC and situated inside the solenoid magnet

3. RPC CALIBRATION PROCEDURE

3.1. MEASUREMENT OF TIME AND CHARGE

Signals from the RPC are split into two streams in a discriminator and splitter module. The first part of the signal is sent directly to a QDC (Charge-to-Digital Converter – CAEN V792) and the second one is discriminated and sent to a TDC (Time-to-Digital Converter – CAEN V775). One QDC bin corresponds to ~ 0.1 pC. The total number of QDC channels is 4096. In order to determine the pedestals of the QDCs for the data taking in the period (May – September 2002) a dozen runs were chosen randomly and based on the data in these runs pedestals were calculated[2]. Pedestal values for 2002 data taking period for each pad are shown on top plot in Fig. 3.

The second stream of RPC signals goes to the TDC module. The TDCs have 4096 channels. The last channels, 4096, is used to keep time-overflow information. The nominal width of one bin according to the manufacturers specifications is 35 ps. This value is only tentative and an additional measurement of the width of each TDC bin is necessary. An example for one pad is

[2] The HARP data acquisition records 100 calibration events in the beginning of every run.

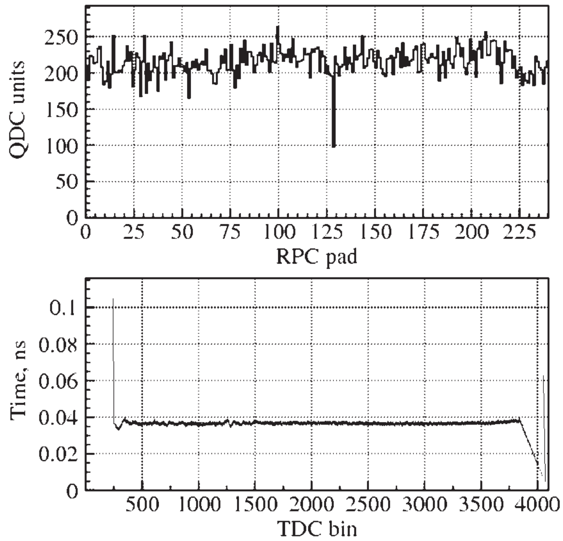

Fig. 3. Top: Pedestals for each RPC pad valid for 2002 data taking period. Bottom: Example of TDC-to-time conversion for one pad

given in Fig. 3 bottom plot. TDC channel to real-time conversion is performed for every pad and for every TDC bin (240*4096 = 983040 numbers in total).

3.2. TIME–CHARGE DEPENDENCE

The part of the RPC signal which goes to the TDC is discriminated by an electronic module, developed especially for the HARP RPC. The discriminator level is fixed and it is just above the white noise. It is observed experimentally that the signals with smaller QDC charges are measured with a larger time than the signals with bigger QDC charges. This is caused by the slower rise of the signals with smaller charges, thus, they exceed the discriminator level later. One can find experimentally what the relation between the recorded TDC time and the pulseheight measured in the QDC is. We call this relation *time–charge dependence.* A typical example is shown in Fig. 4.

During the investigation of the time–charge effect it has been observed that signals from pions and protons have different time–charge behaviour. The origin of this discrepancy is not yet clear, but it is an experimental fact. Our investigations indicate that there is no significant discrepancy between the time–charge dependence of π^- and π^+ signals. We discuss pion and proton time–charge dependencies in following sections.

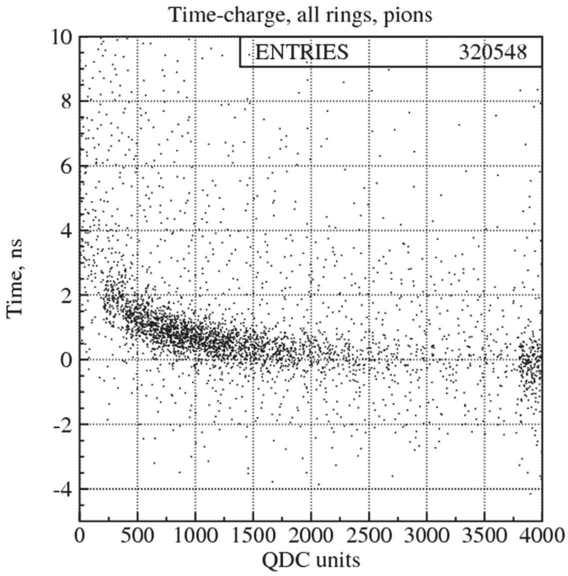

Fig. 4. Time–charge dependence for negative pions. The measured time is larger for smaller QDC charges because of slower rise of the signal. Pions create predominantly charges less than 1500 QDC units. No cuts on the charge measured with the QDC are applied

Pion time–charge correction. We determine an analytical form of the time–charge dependence following the schema below:

1. To select a pure sample of pions and reject $e^{\pm}$, $K^{\pm}$, and protons the measurement of the reconstructed specific energy loss in the TPC (mainly due to the ionization of the TPC gas) is used. Cuts made to select both π^- and π^+ tracks at positive beam momentum of 8 GeV/c and for all targets are shown with solid lines in Fig. 5.
2. Selection of the particle charge. According to HARP signs convention, negative particles have a negative curvature when the beam is of positive charge. In the contrary, positive particles give tracks with positive curvature in positive beams. In combination with the particle identification using the energy loss in the TPC, this selection allows a sample of either π^- or of π^+ to be defined. These samples are sometimes used separately and in other cases combined to increase statistics.
3. TPC track cuts:
   a. TPC points are corrected for static distortions and only first 100 events in the spill are taken to avoid the largest dynamic distortions [6].

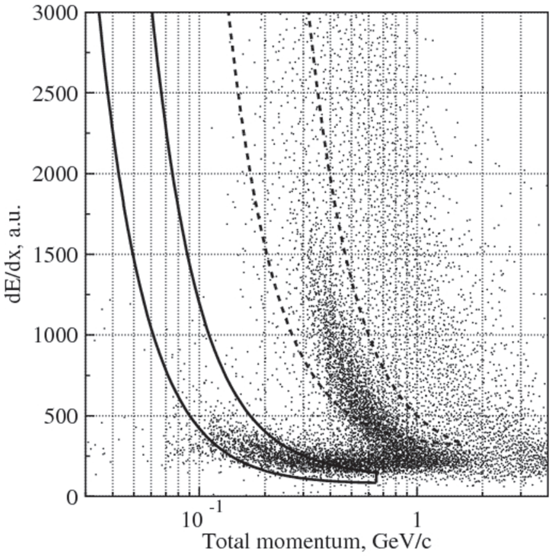

Fig. 5. Cuts for selection of $\pi^{\pm}$ and protons in 'energy loss–total momentum' plane. Pure pion sample is obtained applying two solid lines. The protons are selected through cuts given by two dotted lines

b. Events with reconstructed total momentum higher than 650 MeV/c are rejected (see Fig. 5). Above this momentum the TPC resolution is relatively poor.
c. As an additional protection against the strong time–charge dependence at small charges as well as QDC overflow only events producing charges greater than 300 and less than 3840 QDC units are accepted.
d. Tracks are required to originate from the target and the number of points on the track is required to be ≥ 10. This helps for a better track reconstruction and track length calculation.

4. QDC pedestal subtraction.
5. Time corrections to the TDC measurements:
   a. Raw time (in TDC units) to physical time (in nanoseconds) conversion.
   b. Subtraction of arrival time of the beam particle at the target [7].
   c. Temperature correction of measured time (see section 3.3).
   d. Subtraction of *t*0 constants (see section 3.4). This allows to merge several runs (with different *t*0 constants) and/or to combine different pads in order to increase statistics.
   e. Subtraction of the calculated time-of-flight of pions from the target

to a given RPC pad based on the momentum and track length. The width of the measured time distribution becomes narrower after this operation.

6. Histograms, as in Fig. 4, are filled with already corrected time and QDC charges. We create similar histograms for every RPC pad-ring (one pad-ring includes all pads with the same number within the chamber, *i.e*, we combine 30 pads in one pad-ring; we have 8 pad-rings in total). Histograms per pad contain a small number of events and are not useful. Depending on the available statistics one of the following is done:
   a. In case of sufficient statistics a simple transformation of a given 2-dimensional time–charge distribution into a 1-dimensional presentation is performed. The transformation is realized by replacing the time distribution in each charge bin by its mean value and uncertainty.
   b. If there are not enough events a more complicated procedure is followed. First, slices over the QDC charge distributions are created from the time–charge 2-dimensional histogram and then projected onto the time axis as 1-dimensional histograms. Each 1-dimensional histogram is fitted by a Gaussian function and the fitted mean is taken.
7. All mean values and fitted Gaussian means are put in one histogram as a function of QDC charge and then the histogram are fitted with a polynomial function of the form:

$$t(q) = a_0 + \frac{a_1}{q - q_0} + \frac{a_2}{(q - q_0)^2} + \frac{a_3}{(q - q_0)^3},$$

where *t(q)* is the time in nanoseconds, a, *b, c, d,* and q_0 are parameters that should be determined by the fit, and *q* is the QDC charge.

Such a histogram together with the fit for π^- is shown in Fig. 6 (top curve). The π^+ time–charge dependence is obtained by the same procedure, but for the tracks with positive curvature. Time–charge dependences for both negative and positive pions are quite similar and therefore a combined pion time–charge dependence can be used instead. We create individual time–charge functions for each of the 8 pad-rings.

Proton time–charge correction. In order to obtain the proton time–charge correction a modification is made to the selection described in items 1 and 2 from the previous subsection. To select mainly protons a cut in the measured energy losses of the particles in the TPC gas is applied. The cut is drawn in Fig. 5 as dotted lines. It rejects π^+, e^+ and a fraction of K^+ which is very small in this energy range. From the events in the selected sample we select the protons asking for positive tracks in the TPC. All other steps are the same as in previous subsection. Both pion and proton time–charge corrections are shown in Fig. 6. Proton times are on average ~ 500 ps smaller than the ones of pions. This unexpected effect needs a separate and thorough analysis based on a detailed MC simulation of the interaction processes of the light and heavy charged particles with the RPC detectors in their present design. A theoretical understanding of the pion–proton difference would be difficult to apply in practice in the reconstruction. This is because one first needs to identify the protons before the correct proton time–charge dependence can be used, while the particle identification is expected to be provided just by the RPC detector! On the other hand, the difference in time–charge dependence for protons and pions is not of decisive importance for the data analysis because the main goal of the RPC sub-detector is a separation of pions and electrons. Therefore, only the pion time–charge correction will be used in the RPC calibration procedure and data analysis.

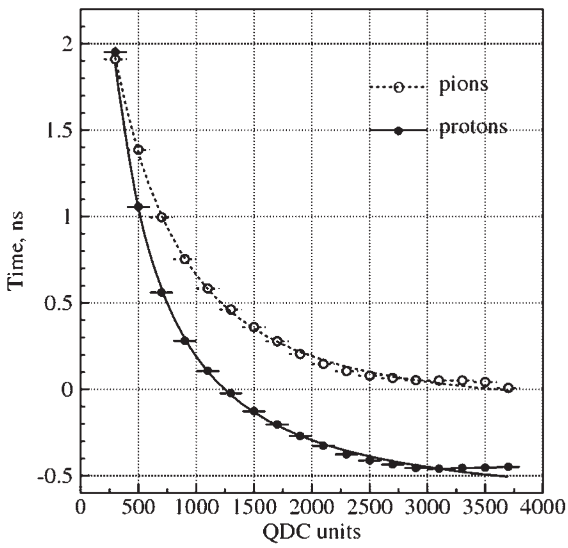

Fig. 6. Time–charge corrections for pions and protons, all pads combined

With the pion time–charge correction the proton time-of-flight appears to be ~ 20% larger on average than the true time for the barrel RPC, and protons are shifted from the theoretical β–momentum curve shown in Fig. 12. Nevertheless, the π–p separation is not spoiled in the considered momentum range, as is evident when p–β plots in Fig. 12 and in Fig. 13 are compared.

The first one is prepared using a different time–charge correction for pions and protons (shown in Fig. 6) and the second one is obtained applying the time–charge correction for pions only to both particle types.

3.3. TEMPERATURE CORRECTION

A potential source of disturbing the proper work of RPC might be the influence of ambient temperature on the RPC and its electronics. The ambient temperature in the vicinity of the RPC detector is measured by a set of sensors. Four of the sensors are mounted between the solenoid magnet and the dipole magnet on the four edges of forward RPC plane. Another group of sensors is located on the barrel RPC – between the outer RPC layer and the water cooling system of the solenoid magnet. This position is a temperature stabilized zone because of the water cooling shield, so the information from this set of temperature sensors is not useful for our purposes.

It was found a linear dependence of the RPC time response on ambient temperature, with a slope of 49±5 ps/deg. It was experimentally observed that within few days the temperature changes more than 10 degree, which leads to time drift larger than 500 ps. This is a very strong effect which must be corrected.

Despite the strong correlation between temperature and time drift another method has been developed which takes automatically into account the temperature drift of measured time. It is shown in [8] that the temperature dependence is not pad specific, thus the time–temperature dependence can be transformed into time–run dependence.

The advantage of this method is that it accounts not only for temperature effects, but also for some other possible shifts of measured time. The procedure we follow is pretty much the same as it has been explained in the section for determination of pion time–charge correction. The next steps are:

1. The measured time-of-flight from all runs and all pads are put into one histogram and the mean of the entries is taken, which gives the integral mean time value for the whole data set;
2. The same procedure is applied for each run, resulting in individual mean time value for that run;
3. The final correction coefficient for each run is the difference between the integral and individual mean time.

Computed this way individual mean times for Ta, Cu, Pb, Sn targets irradiated by 3, 5, and 8 GeV/c positive beam are shown in Fig. 7 (bottom curve, right ordinate). For comparison upper curve and left ordinate represents measured temperatures. Obviously, both curves are strongly correlated.

The comparison of the result of applying run-by-run correction and the case without temperature correction is based on the estimation of the influence of the correction procedure on the t_{tof} resolution (see section 4) . The improvement of the t_{tof} is about 20–30 ps, depending on the pad-ring.

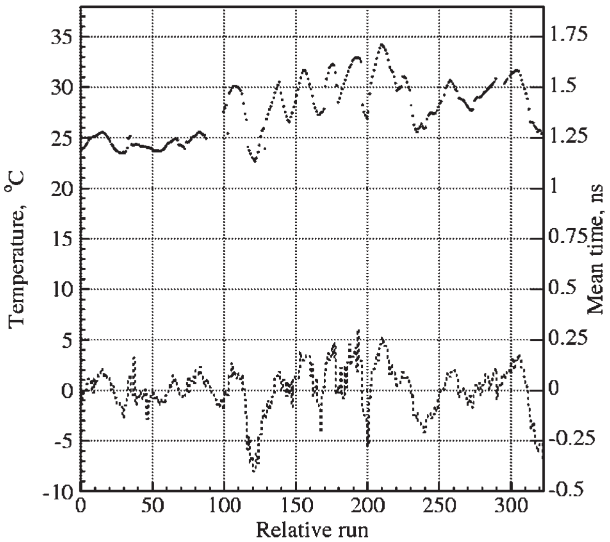

Fig. 7. Run temperature (upper curve, corresponding to left ordinate) and run specific mean time in nanoseconds (bottom curve, corresponding to right ordinate) for thin target. On the x-axis the run numbers are relative

3.4. CALCULATION OF $t0$

The $t0$ constant is defined as a number specific to each pad which, together with the arrival time of the beam particle at the target [7], has to be subtracted from measured RPC time to give the time-of-flight of the secondary particle from the target to the RPC pad. The $t0$ constant absorbs the signal traversing time from the preamplifier to the discriminator (~ 6–7 m of cable), from the discriminator to the TDC module, the processing time of signal in the electronic modules, and similar delays. Our method of obtaining the 240 $t0$ constants is similar to the method used to determine the time–charge correction:

1. Selection of negative TPC tracks. We assume that all such tracks are created by negative pions. This assumption is not fully correct because there is also small fraction of electrons and negative kaons. This is why a dE/dx cut is applied to purify the sample (Fig. 5).
2. TPC track cuts are as explained in section 3.2.

3. RPC pedestal subtraction is performed.
4. The calculation of RPC time contains the following components:
   a. Raw time (in TDC bins) to physical time conversion is performed. The result is time in nanoseconds t_{RPC} .
   b. Time–charge correction t_{charge} is applied.
   c. The arrival time of the beam particle at the target t_{beam} is calculated.
   d. The temperature correction t_{temp} is calculated.
   e. The correction for the transit time of the signal in the pad t_{trans} is done.
   f. The time-of-flight of pions from the target to a given RPC pad tof_{π}, based on the measured track length and track momentum is subtracted.

Finally, the formula for determination of $t0$ looks like:

$$t0 = t_{\text{RPC}} - t_{\text{charge}} - t_{\text{beam}} - t_{\text{temp}} - t_{\text{trans}} - tof_{\pi}$$

5. The above sequence is applied for every RPC pad if the pad is hit during the current event and only one TPC track extrapolates to this pad. Thus we have a $t0$ for each hit. The $t0$'s obtained as described show a Gaussian distribution (see Fig. 8). The fitted mean of the Gaussian is taken as $t0$ constant for each pad individually.

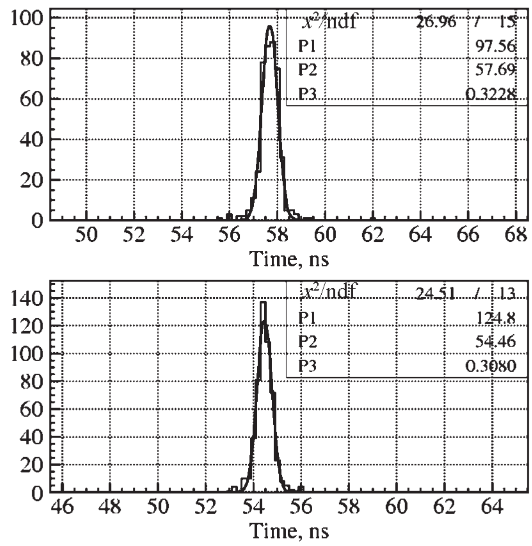

Fig. 8. Examples of *t0* calculation for two RPC pads. The *t0* for a given pad is the mean of the Gaussian fit

The determination of $t0$ constants is a more delicate operation compared, for example, to the time–charge correction or pedestal subtraction, which are stable during the data-taking time. The ingredients of $t0$ constants are very sensitive to wide number of accidental factors, which might appear and disturb the normal data taking process in time intervals with different duration. Because of the requirement for statistical reliability it is impossible to compute the $t0$ constants by a small number of runs closed in a short time interval. But a compromise solution is computation of $t0$ constants for a single experimental setting[3]. In certain cases a higher precision of $t0$ constants might be achieved by a combination of few settings taken within short time period.

4. OVERALL RPC PERFORMANCE

In this section we describe the current state of RPC performance, namely the intrinsic RPC time resolution, combined RPC, TPC and BEAM time resolution and RPC particle identification capabilities.

4.1. TIME RESOLUTION

In order to estimate the intrinsic RPC time resolution we use the fact that there is a small region of overlap of the RPC layers as shown in Fig. 2. The active volume of the overlap is ~ 20%. This geometrical feature allows us to estimate the intrinsic RPC time resolution independently on the TPC tracking capabilities.

For the determination of the RPC time resolution we use tracks selected according to rules described in the previous sections, requiring in addition that they cross the areas of overlap of the pads. The intrinsic RPC time resolution can be extracted from the distribution of differences of time-of-flight for one and the same track that crosses the region of overlap and gives signals in both pads. The major correction in the time-of-flight computation is caused by the time–charge dependence. In the present study only the pion time–charge correction is used. Because of statistical reasons we accumulate histograms for time differences not per pad, but per pad-ring. The difference of these times has a distribution that can be partially fitted by a Gaussian function with a sigma that varies from at about 300 ps to 280 ps. Assuming an equal time resolution of the pads belonging to a given pad-ring the above numbers should be divided by a factor $\sqrt{2}$ to obtain the intrinsic resolution of a single RPC pad-ring. An example is shown in Fig. 9.

[3] According to the HARP convention "setting" means certain combination of a type and beam energy, target characteristics, apparatus tuning, etc.

The intrinsic time resolution as a function of RPC pad-ring is given in Fig. 10 (the numbers already include the division by $\sqrt{2}$). One can easy conclude that the time resolution is worse for bigger charges. This dependence of the time resolution is unexpected. Most likely bigger charges have different behaviour during a transportation in the pad compared to smaller ones. Another possible reason are hits producing bigger charges and caused by multiple tracks crossing the pads. Such tracks might be generated by fast particles obtained in accompanying nuclear reactions induced in the technological detector materials by secondary particles stemming from the target. These tracks are omitted from the analysis because they do not satisfy the selection criteria as enumerated in section 3.2. Actually, to get deeper understanding of this problem more detailed studies based on correct MC simulations or special test measurements are needed.

However, this effect is not critical because only a small fraction, (of the order of few percent) of the particles creates such big charges. The best improvement for rings 5, 6 and 7 is observed when larger charges are rejected. This is due to the fact that the deposited charge is bigger for downstream rings which is a pure geometrical effect. The average intrinsic time resolution is less than 200 ps in both cases shown.

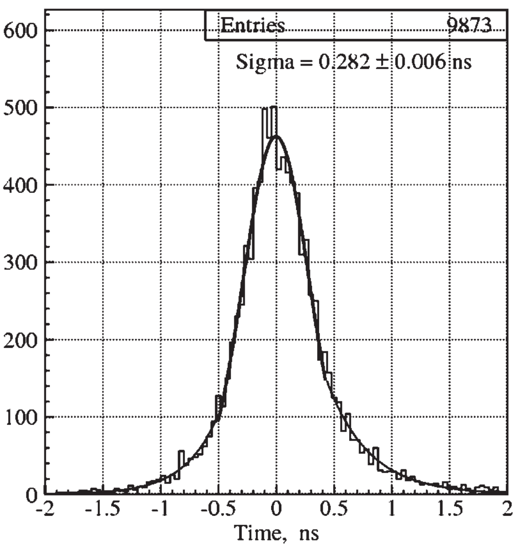

Fig. 9. Time difference for overlapping pads in pad-ring 4. The distribution is fitted by a Gaussian (solid curve) and two exponential functions. The sigma shown is not divided by $\sqrt{2}$

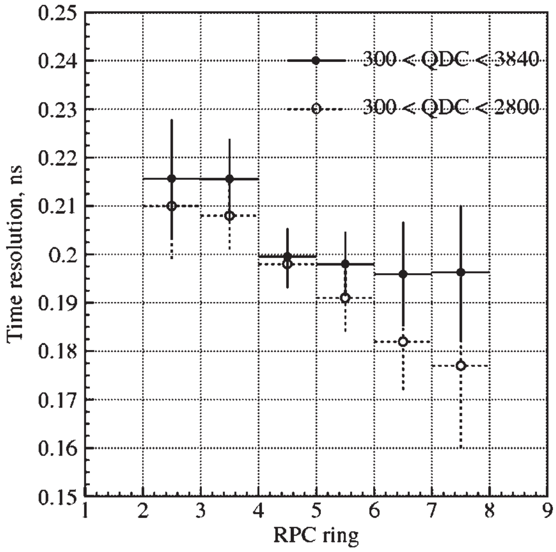

Fig. 10. Intrinsic RPC time resolution versus ring number for two ranges of QDC charges. The division by $\sqrt{2}$ is executed. The average value is ~ 200 ps. First and last rings are excluded from the plot, because of low statistics

The RPC sub-detector is built not to work independently from the other detectors. Moreover, its design task is to give complementary information to that of the TPC, the main large-angle detector. The calibration of the RPC and the RPC data analysis is not possible without TPC and without BEAM detectors. As described in section 3, we use reconstructed TPC tracks to obtain time–charge correction, $t0$ constants, etc. The uncertainty of t_{tof} (see section 3.4) includes not only the RPC intrinsic time resolution, but also the reflection of the quality of the TPC track parameters (trough tof_{π}), and beam particle arrival time t_{beam} . One can express the t_{tof} uncertainty as:

$$\sigma^2(t_{\text{tof}}) = \sigma^2(t_{\text{RPC}}) + \sigma^2(t_{\text{TPC}}) + \sigma^2(t_{\text{beam}}),$$

where $\sigma(t_{tof})$ is the t_{tof} uncertainty, $\sigma(t_{\text{RPC}})$ is the intrinsic RPC time resolution, determined to be ~ 200 ps; $\sigma(t_{\text{TPC}})$ is the ‘time resolution’ of TPC tracks[4]. It is difficult to estimate this uncertainty directly. The quantity $\sigma(t_{\text{beam}})$ is the uncertainty of the arrival time of beam particle at the target. This uncertainty is estimated to be ~70 ps [7].

An example of t_{tof} uncertainty for two pads is given in Fig. 8. In those

[4] The uncertainties included in this value are those of the reconstructed momentum by the TPC, the quality of the track extrapolation to the respective RPC layer and the calculation of the track length.

cases the overall time resolution is 323 ps and 308 ps. In Fig. 11 the averaged over all 30 pads in a ring t_{tof} uncertainty versus RPC ring number for three charge ranges is shown. It varies from 320 to 350 ps for the case when $300 \leq \mathrm{QDC} \leq 3840$.

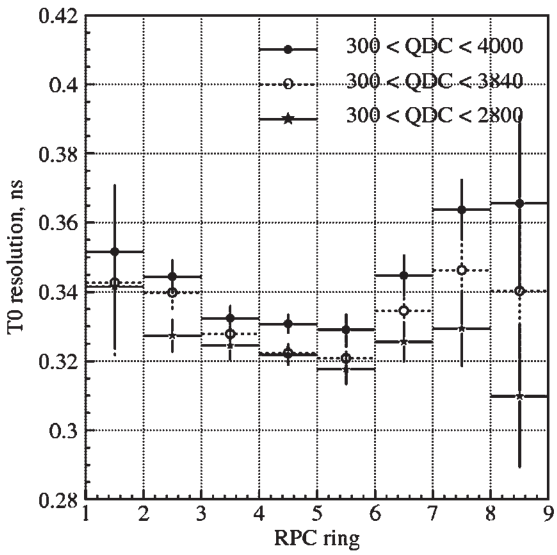

Fig. 11. t_{tof} uncertainty versus RPC ring number for different QDC charge ranges. The average value is ~ 330 ps. It represents combined time resolution of RPC, TPC and BEAM detectors

Using the above formula one can calculate that the contribution of the TPC to the time resolution is about 250 ps, on average, which is higher than the intrinsic RPC resolution.

4.2. PARTICLE IDENTIFICATION CAPABILITIES

The particle identification capabilities of combined TPC–RPC system have been evaluated after applying the calibration procedure described above. We used a sample of tracks obtained by the 8 GeV/c beam impinging on thin Cu, Ta and Pb targets. Fig. 12 demonstrates the correlation between the measured relativistic velocity β of all particles and their total momentum when the pion time–charge correction is used. The shift of the protons curve relative to the theoretical curve is due to specific time–charge dependence for protons as explained in section 3.2. Similar picture is given for all particles in Fig. 13, where individual time–charge corrections for pion and protons are applied. The $e^{\pm}/\pi^{\pm}$ separation capabilities are better seen in Fig. 14, where the distribution of measured β, is shown for different momenta slices. Similar pictures are given for proton/pion separation in Fig. 15.

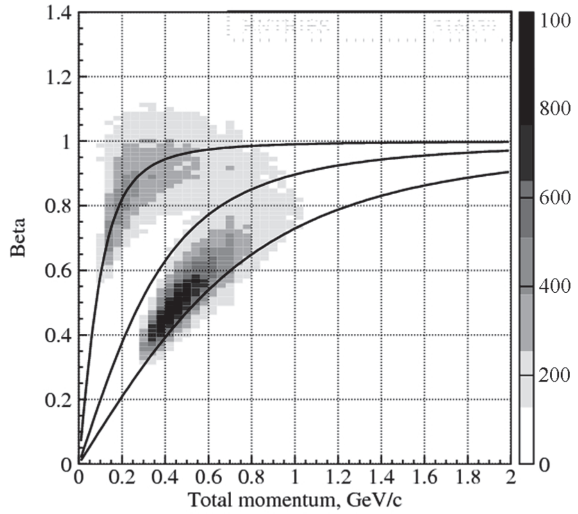

Fig. 12. The relativistic velocity β, measured by the RPC, as a function of momentum, measured by the TPC, for positive particles. The curves represent theoretical dependence for pions (upper curve), kaons (middle curve) and protons (bottom curve)

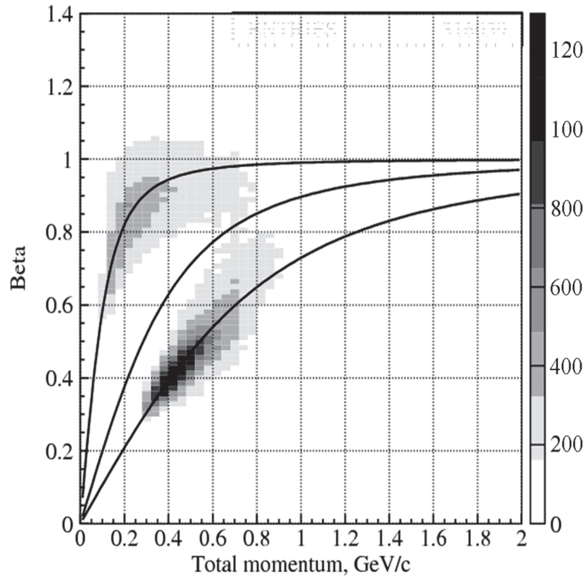

Fig. 13. The relativistic velocity β, measured by the RPC, as a function of momentum, measured by the TPC, for all particles. Individual time–charge corrections are applied for pions and protons. The protons are centred on the theoretical (bottom) curve

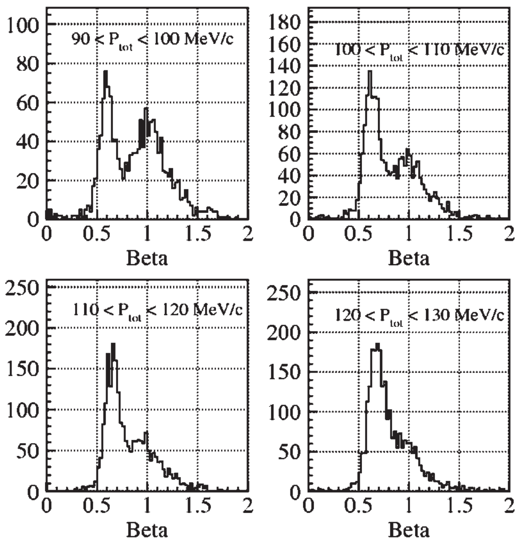

Fig. 14. The relativistic velocity β in different momentum slices for all particles. Top left: 90 ≤ momentum ≤ 100 MeV/c: $e^{\pm}$ peak is centred at $\beta = 1$; $\pi^{\pm}$ peak appear at $\beta \sim 0.6$. Top right: 100 ≤ momentum ≤ 110 MeV/c: the fraction of $\pi^{\pm}$ rises and $e^{\pm}$ decreases. Bottom left: 110 ≤ momentum ≤ 120 MeV/c: $\pi^{\pm}$ peak becomes dominant. Bottom right: 120 ≤ momentum ≤ 130 MeV/c: it is already difficult to separate $\pi^{\pm}$ from $e^{\pm}$

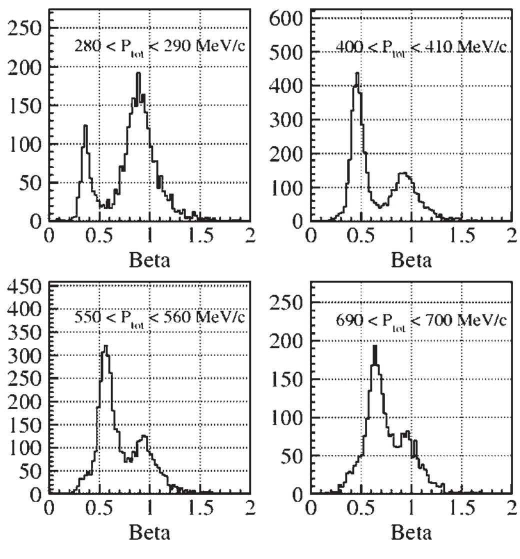

Fig. 15. Relativistic velocity β in different momentum slices for all particles. Top left: 280 ≤ momentum ≤ 290 MeV/c: $\pi^{\pm}$ peak is dominant, centred at $\beta \sim 0.9$; protons appear at $\beta \sim 0.35$. Top right: 400 ≤ momentum ≤ 410 MeV/c: the proton peak rises and becomes dominant. Bottom left: 550 ≤ momentum ≤ 560 MeV/c: the proton peak is moving to to larger β. Bottom right: 690 ≤ momentum ≤ 700 MeV/c: $\pi^{\pm}$ and protons are slowly merging into one peak

5. CONCLUSION

After a short introduction in goals and detector system of the HARP experiment, we describe in details the HARP RPC time-of-flight system. Various effects as time–charge and temperature dependence, have been studied, understood, parametrized and coded. The intrinsic RPC time resolution in order of 200 ps and overall time resolution of 330 ps have been obtained. RPC particle identification capabilities are demonstrated.

REFERENCES

1. Catanesi, M.G. et al., HARP Collaboration. CERN-SPSC, **99-35**, 1999.
2. Ahn, M.H. et al., K2K Collaboration. *Phys. Rev. Lett.*, **90**, 2003, 041801.
3. Stancu, I. et al., MiniBooNE Collaboration. **FERMILAB-TM-2207**, 2001.
4. Agostinelli, S. et al. *NIM*, **A506**, 2003, 250.
5. Bogomilov, M. et al. *NIM*, **A508**, 2003, 152.
6. Borghi, S., S. Giani. HARP Memo, **04-004**, 2004.
7. Schmitz, D. HARP Memo, **04-003**, 2003.
8. Artamonov, A. et al. HARP Memo, **05-004**, 2004.

Received December 2005

Mariyan Bogomilov
St. Kliment Ohridski University of Sofia
Faculty of Physics
Department of Atomic Physics
5, James Bourchier Blvd.
1164 Sofia, Bulgaria
E-mail: marian@phys.uni-sofia.bg